Kinetic Monte Carlo method for dislocation migration in the presence of solute

Chaitanya S. Deo
Princeton Materials Institute, Princeton University, Princeton, New Jersey 08540, USA
and Department of Materials Science and Engineering, University of Michigan, Ann Arbor, Michigan 48105, USA

David J. Srolovitz
Department of Mechanical and Aerospace Engineering, Princeton University, Princeton, New Jersey 08544, USA
and Princeton Materials Institute, Princeton University, Princeton, New Jersey 08544, USA

Wei Cai and Vasily V. Bulatov
Chemistry and Materials Science Directorate, Lawrence Livermore National Laboratory, Livermore, California 94550, USA
(Received 21 April 2004; published 6 January 2005)

We present a kinetic Monte Carlo method for simulating dislocation motion in alloys within the framework of the kink model. The model considers the glide of a dislocation in a static, three-dimensional solute atom atmosphere. It includes both a description of the short-range interaction between a dislocation core and the solute and long-range solute-dislocation interactions arising from the interplay of the solute misfit and the dislocation stress field. Double-kink nucleation rates are calculated using a first-passage-time analysis that accounts for the subcritical annihilation of embryonic double kinks as well as the presence of solutes. We explicitly consider the case of the motion of a ⟨111⟩-oriented screw dislocation on a {011}-slip plane in body-centered-cubic Mo-based alloys. Simulations yield dislocation velocity as a function of stress, temperature, and solute concentration. The dislocation velocity results are shown to be consistent with existing experimental data and, in some cases, analytical models. Application of this model depends upon the validity of the kink model and the availability of fundamental properties (i.e., single-kink energy, Peierls stress, secondary Peierls barrier to kink migration, single-kink mobility, solute-kink interaction energies, solute misfit), which can be obtained from first-principles calculations and/or molecular-dynamics simulations.

DOI: 10.1103/PhysRevB.71.014106 PACS number(s): 61.72.Lk, 61.72.Bb, 02.70.Uu, 61.82.Bg

I. INTRODUCTION

The principal mechanisms of crystal plasticity involve the motion of crystal defects of different dimensionality. These defects include point defects (e.g., vacancies, self-interstitials), line defects (dislocations), planar defects (e.g., twins), and volumetric defects (e.g., resulting from martensitic transformations). Plasticity in most metallic alloys is a macroscopic manifestation of dislocation activity, except at very high temperature and small stress. Dislocations glide along crystal planes (glide planes), cross-slip, or climb onto other glide planes and interact with each other and with other defects within the crystal. The plastic response of metals is typically the result of the motion of a large number of dislocations.

Dislocation dynamics (DD) simulations (e.g., see Bulatov *et al.*,[1,2] Gomez Garcia *et al.*,[3] Tang *et al.*,[4] and Zbib *et al.*[5]) model the motion and interaction of a large number of dislocations and their influence on the mechanical properties of crystals. These simulations treat the dislocations as line segments connected through nodes. The dynamics of dislocation motion is thus reduced to the dynamics of the nodes and depends on the driving forces (elastic or chemical) acting upon the dislocations. The elastic interactions between dislocations occur over large distances and are relatively complex. The simulation of the motion of a large number of dislocations over physically meaningful time scales is a major computational bottleneck for DD simulations. In alloys, dislocation dynamics is further complicated by the interactions of dislocations with solute atoms (solute atoms interact elastically with dislocations and modify the dislocation core).

In order to simulate a large number of dislocations for reasonable lengths of time, DD simulations employ simple rules that dictate the motion of the dislocations. These mobility rules prescribe the relationship between the velocity of a dislocation and the forces acting upon it. The forces may arise from the applied stress, elastic self-interactions, dislocation-dislocation interactions, and, in the case of alloys, interactions with solute atoms. The relationship between dislocation velocity and force is commonly described via power laws[6,7] or exponential[8,9] relationships. The reliability with which the DD simulations mimic the plastic behavior of the crystal depends on the accuracy of these mobility rules.

Quantitative experimental information on the intrinsic mobility of individual dislocations is rare. On the other hand, first-principles calculations and atomic-level simulations such as molecular dynamics[49–52] (MD) may be utilized to obtain some of the energetics of dislocation motion. However, determination of dislocation force-velocity (mobility) relations from simulations requires tracking the dynamics of individual dislocations over relatively long time scales ($\sim\mu$s). Given the inherently small time scales of MD (10^{-12} s), such simulations are rarely possible today.

Kinetic Monte Carlo (KMC) methods[10–12] provide a bridge between the large-scale dislocation dynamics simulations of crystal plasticity behavior and the atomic-scale

simulation of dislocations that can be used to determine the mobilities of dislocations. These KMC methods use information on the energetic barriers to atomic hopping or kink migration that control the motion of a dislocation in order to obtain the relationships between the velocity of the dislocation and the driving forces acting upon it. This information can provide the requisite input to mesoscale dislocation dynamics simulations.

Several researchers have performed kinetic Monte Carlo simulations of dislocation motion via kink migration. These simulations were based upon the assumption that dislocations are an ensemble of pure screw and edge segments. Rates of the fundamental processes in kink migration-controlled dislocation dynamics (i.e., kink pair nucleation, lateral kink migration, and kink-kink annihilation) were determined and a KMC procedure was employed to select between these types of events at each simulation step. These models incorporated the long-range elastic interactions between the kinks,[8] rather than simply using the line tension approximation employed in most continuum models.[13] Lin and Chrzan[14] performed KMC simulations of the dislocation migration in Ta as a function of temperature and applied stress by mapping the edge and screw segments onto a fixed lattice. Cai *et al.* employed a similar KMC method for simulating the motion of two partial dislocations in Si (Ref. 15) and a single $\langle 111\rangle$-oriented screw dislocation in Mo.[16,17] The screw dislocation in Mo was allowed to move on all three available $\{110\}$ glide planes that comprised the $\langle 111\rangle$ $\{110\}$ slip system. All these studies were focused on dislocation mobility in pure crystals.

Since engineering materials are never pure, this study focuses upon dislocation motion in a solid solution alloy at low temperature. In particular, we employ a KMC method to simulate the motion of screw dislocations in a substitutional, solid solution alloy. The dislocation moves by the kink mechanism—double-kink nucleation, kink migration, and annihilation. The dislocation is constrained to move on a glide plane (i.e., cross-slip and climb are not considered), while the solutes are distributed randomly in three dimensions. We first provide a detailed description of the simulation model and then apply this model to determine the influence of temperature, applied stress, and solute concentration on the velocity of a $\langle 111\rangle$-oriented screw dislocation in Mo with substitutional solute.

II. SIMULATION MODEL

In the present simulation, we model the glide of a dislocation on a plane, while the solute is distributed in three dimensions. The dislocation has, on average, a screw orientation, but consists of screw and edge dislocation segments. This model does not allow for cross-slip of the screw segments or climb of the edge segments.

A. Kink model of dislocation motion

The dislocation is assumed to move via a kink mechanism—this involves the nucleation of pairs of kinks of opposite sign, kink migration, and the mutual annihilation of oppositely signed kinks. Elastic theory for kink formation and diffusion as a mechanism for dislocation motion was first developed by Eshelby[18] and Seeger *et al.*[19–21] and has been reviewed in detail by Hirth and Lothe.[8] The Monte Carlo simulation samples a list of different classes of possible kink nucleation and migration events. Kink-kink annihilation is considered as a special case of kink migration.

Kinks nucleate in oppositely signed pairs. The kinks on a screw are of edge type and vice versa. Following Hirth and Lothe,[8] the nucleation rate for a double kink of width $1b$ (where b is the Burgers vector) is

$$j_{dk} = \omega \exp\left(-\frac{2E_k + W_{\text{int}} - \tau_{\text{eff}} b^2 h/2}{k_B T}\right), \tag{1}$$

where ω is the attempt frequency factor, E_k is the energy of an isolated kink, W_{int} is the interaction energy between the two kinks in the pair, h is the kink height, $k_B T$ is the thermal energy, and τ_{eff} is the local resolved stress that includes the applied stress, the stress field of the solutes, and the self stress field associated with the screw segments. Hirth and Lothe calculate the interaction energy W_{int} depending on the separation between (edge segments) kinks z_k as[8]

$$W_{\text{int}} = -\frac{\mu h^2}{8\pi z_k b}\left(b_z^2 \frac{1+\nu}{1-\nu} + b_x^2 \frac{1-2\nu}{1-\nu}\right), \tag{2}$$

where the nominal orientation of the dislocation line is along z, b_x and b_z are the x and z components of the burgers vector, μ is the shear modulus, and υ is Poisson's ratio.

The energy of the isolated kink, E_k, may be obtained from atomistic simulations. For example, Xu and Moriarty[22] used atomistic simulations employing empirical many-body potentials for a kink on a $\langle 111\rangle$-oriented screw dislocation in Mo and found that $E_k \approx 1$ eV. The entire numerator in the exponential in Eq. (1) is referred to as the kink pair energy[19–21] or as the double-kink energy E_{dk} (Ref. 8). Nucleation of a double kink in the presence of a solute depends on the solute-core interactions. In the present study, we assume that a solute atom is an obstacle to kink migration (i.e., it provides an additional, localized barrier E_b to kink motion).

A kink, once formed, can migrate along the dislocation line until it meets a kink of opposite sign and annihilates. The rate of migration of the kinks depends on the magnitude of the secondary Peierls barrier, W_m (i.e., the activation energy for kink motion). If the secondary Peierls barrier is very large (e.g., in the case of Si) or if kink motion is hindered by a solute atom, the migration rate (or kink diffusivity) is given by the following expression:[8,15]

$$j_m = \omega \exp\left(-\frac{W_m - \tau_{\text{eff}} b^2 h/2}{k_B T}\right). \tag{3}$$

Kink mobility in the presence of a solute atom also depends on the solute-core interactions. As in the case of double-kink nucleation, we assume that the solute increases the activation barrier for kink diffusivity by an amount proportional to the local solute barrier E_b.

If the secondary Peierls barrier for the kink motion is very small in the absence of solute [$\sim$0.0005 eV for a $\langle 111\rangle$ screw dislocation in Mo (Refs. 16,17)], the kink diffusivity is

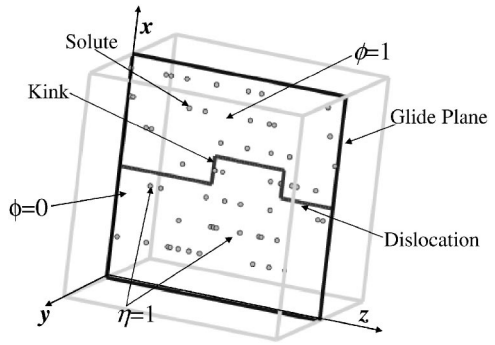

FIG. 1. Illustration of the dislocation-solute model. The order parameter is defined over the glide plane and is used to identify the location of the dislocation. The solute atoms are distributed in three dimensions and are represented by a field (see text for details).

very large. In such cases, the kink migration is not thermally activated but is characterized by a lattice damping (drag) coefficient B_k, which is dominated by phonon drag. In such a case, the kink velocity v_k is proportional to the driving force experienced by the kink:[9]

$$v_k = \frac{\tau_{\text{eff}}}{B_k} b, \tag{4}$$

where τ_{eff} is the total stress. When the kink is adjacent to a solute atom, we describe the motion of the kinks using Eq. (3) and otherwise use Eq. (4).

B. Geometric description of the dislocation and solute

The simulation cell is represented as a three-dimensional (3D) simple cubic lattice (see Fig. 1), where the dislocation glide plane has normal $\hat{y}$ (at position $y=0$). The Burgers vector $\vec{b}$ is parallel to the z direction, as are the screw segments. The spacing in the x and z directions is governed by the nature of the dislocation being modeled. For example, in modeling a screw dislocation in Mo, we assume that the Burgers vector is of the $\langle 111 \rangle$ type and, hence, the z direction in the simulation lattice corresponds to a $\langle 111 \rangle$ direction in the crystal. The simulation cell lattice spacing in the z direction is $b=\sqrt{3}a_0/2$, the lattice spacing in the x direction is $h=a_0\sqrt{2/3}$, and the spacing between the $\{110\}$ glide planes is $l=a_0/\sqrt{2}$. An order parameter $\phi(x_i,0,z_i)$ is defined over the glide plane and is used to identify the location of the dislocation:

$$\phi(x_i,0,z_i) = \begin{cases} 1, & (x_i,0,z_i) \text{ is part of slipped glide plane,} \\ 0, & (x_i,0,z_i) \text{ is part of unslipped glide plane.} \end{cases} \tag{5}$$

A dislocation line segment lies between any pair of nearest-neighbor (square) lattice points in the glide plane that have different values of ϕ.

The solute atoms are distributed in three dimensions and are represented by a field $\eta(x_i,y_i,z_i)$ which is one at lattice points occupied by solute atoms and zero otherwise. The solute atoms within $\sqrt{2}a_0$ of the glide plane interact directly with the dislocation core [this corresponds to five (110) planes in the simulation lattice]. Using the geometric scheme proposed above, we can describe the positions of all dislocation segments and solutes in sufficient detail to model dislocation motion in the presence of solutes via a kink model.

C. Dislocation self-stress

A dislocation creates a stress field that produces forces on other dislocations and results in interaction between the dislocation and solute atoms. The self-stress of a dislocation is the stress exerted on a dislocation segment by all other dislocation segments. Many earlier approaches accounted for the self-stress effect by replacing the dislocation line with a smooth curve with finite line tension (it is the line tension that models the self-stress). This simple approximation implies that the free energy of the dislocation is simply proportional to the dislocation length $\mathcal{L}$, with a constant of proportionality equal to the dislocation line energy.[8,13] This approximation does not account for the true, nonlocal nature of the interaction between dislocation segments and is clearly inapplicable in many circumstances, such as where the variations in dislocation line curvature are large. Further, the force on a dislocation line segment, in the line tension approximation, is independent of the location of all other dislocation line segments and only depends on the local line curvature.

In our model, every dislocation configuration is represented by an ensemble of straight line segments in the geometric scheme described above. The stress field associated with a segmented dislocation of arbitrary shape can be calculated everywhere as a summation of the stress fields associated with each segment, as described below. The accuracy of this approach depends upon the applicability of an edge and screw segment decomposition of the dislocation shape and the length scale of these segments. The computational work associated with calculating the stress field along the entire dislocation line increases as the square of the total length of the dislocation line. Because of this overhead, simulations of dislocation dynamics that properly account for dislocation self-interactions have not been performed until recently.[23] A similar approach was recently proposed for describing dislocation motion in silicon[15] and pure molybdenum[16,17] within the kinetic Monte Carlo framework.

We employ the approach proposed by Hirth and Lothe[8] to calculate the stress field of a dislocation configuration (represented by a sequence of straight line segments) as a summation of the stress fields of the individual segments. For a general segmented dislocation configuration, the stresses of the individual line segments can be transformed as tensors to a common coordinate system and summed to give the total physical stress. To calculate the stresses of the individual line segments, the coordinate system shown in Fig. 2(a) is adopted, where the dislocation line segment lies along the z axis. Following Hirth and Lothe,[8] the stresses at an arbitrary point $\vec{r}(x,y,z)$ due to the segment (z'_A,z'_B) with a Burgers vector $\vec{b}=(b_x,b_y,b_z)$ are obtained by integrating along the segment from z'_A to z'_B, yielding

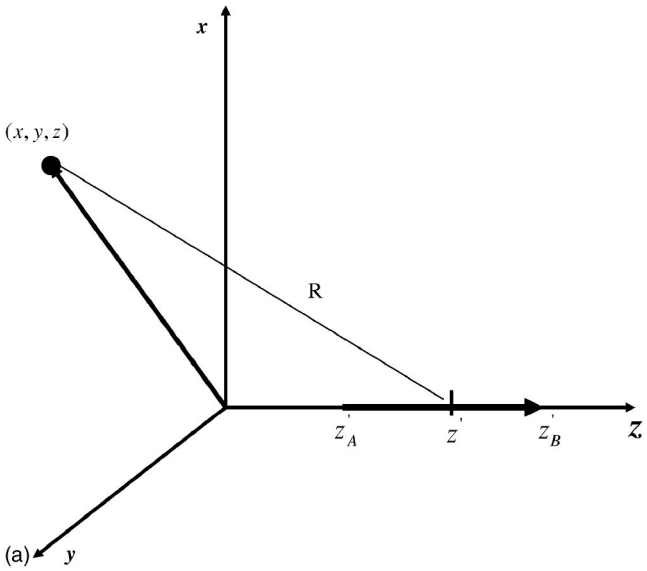

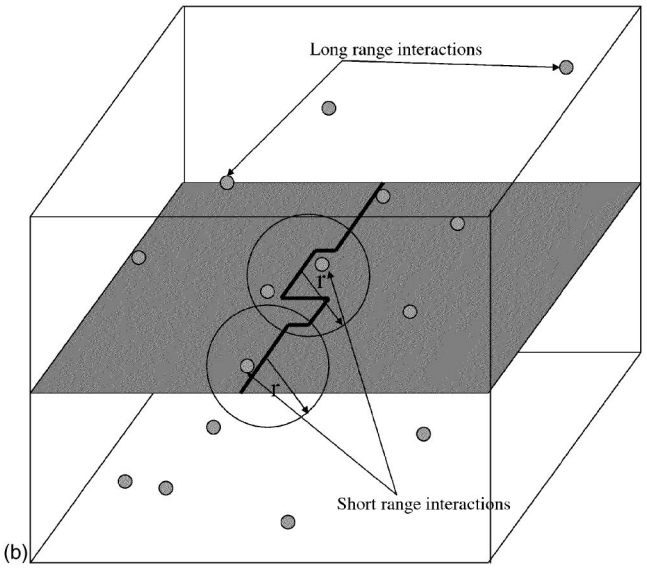

FIG. 2. (a) Schematic illustration of the interaction between a dislocation segment (z_A', z_B') and a point (x,y,z) in the simulation cell. The stress field due to the dislocation segment is described in the text. (b) Schematic illustration of the short-range and long-range interactions between the dislocation and the solute atoms. The solute atoms are distributed in three dimensions around the dislocation.

$$\sigma_{ij} = \sigma_{ij}(z_B') - \sigma_{ij}(z_A'), \tag{6}$$

where $\sigma_{ij}(z')$ is obtained as

$$\frac{\sigma_{xx}(z')}{\sigma_0} = b_x \frac{y}{R(R+\lambda)}\left[1 + \frac{x^2}{R^2} - \frac{x^2}{R(R+\lambda)}\right] + b_y \frac{x}{R(R+\lambda)} \times \left[1 - \frac{x^2}{R^2} - \frac{x^2}{R(R+\lambda)}\right], \tag{7a}$$

$$\frac{\sigma_{yy}(z')}{\sigma_0} = -b_x \frac{y}{R(R+\lambda)}\left[1 + \frac{y^2}{R^2} - \frac{y^2}{R(R+\lambda)}\right] - b_y \frac{x}{R(R+\lambda)}\left[1 + \frac{y^2}{R^2} + \frac{y^2}{R(R+\lambda)}\right], \tag{7b}$$

$$\frac{\sigma_{zz}(z')}{\sigma_0} = -b_x\left[\frac{2\nu y}{R(R+\lambda)} + \frac{y\lambda}{R^3}\right] + b_y\left[\frac{2\nu x}{R(R+\lambda)} - \frac{x\lambda}{R^3}\right], \tag{7c}$$

$$\frac{\sigma_{xy}(z')}{\sigma_0} = -b_x \frac{x}{R(R+\lambda)}\left[1 - \frac{y^2}{R^2} - \frac{y^2}{R(R+\lambda)}\right] + b_z \frac{y}{R(R+\lambda)}\left[1 - \frac{x^2}{R^2} - \frac{x^2}{R(R+\lambda)}\right], \tag{7d}$$

$$\frac{\sigma_{yz}(z')}{\sigma_0} = b_x\left[\frac{\nu}{R} - \frac{y^2}{R^3}\right] + b_y \frac{xy}{R^3} - b_z \frac{x(1-\nu)}{R(R+\lambda)}, \tag{7e}$$

$$\frac{\sigma_{xz}(z')}{\sigma_0} = -b_x \frac{xy}{R^3} + b_y\left[-\frac{\nu}{R} - \frac{x^2}{R^3}\right] + b_z \frac{y(1-\nu)}{R(R+\lambda)}, \tag{7f}$$

$$\sigma_0 = \frac{\mu}{4\pi(1-\upsilon)}, \quad R = \sqrt{x^2 + y^2 + (z-z')^2}, \quad \lambda = z' - z. \tag{7g}$$

Equations (6) and (7) can be applied to each dislocation segment by suitable rotation and translation of the coordinate axes in Fig. 2(a) and the total self-stress at any point obtained by summing over all segments.

In the geometry of the present simulations, we choose $\overline{b} = (0,0,b_z)$ and constrain the dislocation to lie only on the $y=0$ glide plane. The dislocation segment length (a) is b or h for a screw or edge component, respectively. In the coordinate system in which the dislocation segment is centered at the origin and extends along the z axis, the stress at any point is given by Eq. (6) with the stresses

$$\frac{\sigma_{xy}(z')}{\sigma_0} = \begin{cases} -b_x \dfrac{x}{R(R+\lambda)}, & z < z_1' < z_2', \\ -b_x \dfrac{\lambda}{xR}, & z_1' < z < z_2', \\ -b_x \dfrac{x}{R(R-\lambda)}, & z_1' < z_2' < z, \end{cases} \tag{8a}$$

and

$$\frac{\sigma_{yz}(z')}{\sigma_0} = \begin{cases} b_x \dfrac{\upsilon}{R} - b_z \dfrac{x(1-\upsilon)}{R(R+\lambda)}, & z < z_1' < z_2', \\ b_x \dfrac{\upsilon}{R} - b_z \dfrac{\lambda}{xR}, & z_1' < z < z_2', \\ b_x \dfrac{\upsilon}{R} - b_z \dfrac{x(1-\upsilon)}{R(R-\lambda)}, & z_1' < z_2' < z. \end{cases} \tag{8b}$$

These expressions for the stresses associated with individual segments were first used in KMC simulations of dislocation motion by the kink mechanism in silicon[15] and pure molybdenum.[17] The self-stress associated with all of the dislocation segments and the applied stress and stresses from

the solutes make up the total stress τ_{eff} which is used to calculate double-kink nucleation rates [Eq. (1)] and kink diffusivities [Eqs. (3) and (4)].

D. Solute dislocation interactions

Solute atoms interact with the dislocation both through their long-range stress field and through their direct interactions with the dislocation core. The long-range component of the solute-dislocation interaction contributes to τ_{eff} and hence to the double-kink nucleation and kink migration rates. The long-range stress field of the solute atoms is treated by modeling them as point sources of dilatation for which

$$\sigma_{rr} = -\frac{\mu}{\pi}\frac{\delta\nu}{r^3}, \quad \sigma_{\theta\theta} = \sigma_{\phi\phi} = \frac{\mu}{2\pi}\frac{\delta\nu}{r^3}, \tag{9}$$

where $\delta\nu$ is the magnitude of the dilatation. We define the solute-dislocation interactions as short-range or long-range depending on the distance $|r|$ of the solute from the dislocation segment [as shown in Fig. 2(b)]. If the solute is far away from the dislocation—i.e., $|r| > \sqrt{2}a_0$—the stress field is calculated using Eq. (11) and added to the total stress that acts on the dislocation segment. If the solute is near the dislocation—i.e., $|r| < \sqrt{2}a$—the solute interacts with the core of the dislocation. We assume that such a core-solute interaction provides a barrier of $W_m = E_b$ to the motion of the kink [see Eq. (3)].

E. Double-kink nucleation

Of the unit processes in the kink diffusion model, nucleation of kink pairs is the slowest and, hence, plays an important role in determining both the velocity of the dislocation and the efficiency of the KMC simulation. The energy barrier that must be overcome in order to nucleate a double kink on a straight screw dislocation is calculated using the following expression:[8]

$$\Delta E = 2E_k - \frac{\mu b^2 h^2}{8\pi w}\left(\frac{1+\nu}{1-\nu}\right) - \frac{\sigma b h w}{2}, \tag{10}$$

where E_k is the energy of an isolated kink, w is the double-kink width (kink-kink separation), σ is the effective applied stress (see above), h is the kink height, and μ is the shear modulus. The first term is the energy to form two isolated kinks on an otherwise straight dislocation and is positive. The second term is the kink-kink interaction [i.e., the second term in Eq. (12)] and is always negative. The last term is the interaction of the kinks with the long-range stress field (this excludes elastic interactions between kinks) and can be of either sign. The double-kink energy is plotted in Fig. 3(a) for an applied stress of $0.1\tau_P$, where τ_P is the Peierls stress and all parameters were chosen to correspond to a screw dislocation in Mo ($\tau_P = 0.0025\mu, \mu = 12.3 \times 10^4$ MPa, $E_k = 1$ eV).[24,25] The double-kink energy increases with increasing double-kink width at small kink separations and decreases after a critical double-kink width. The critical double-kink width (i.e., above which the double-kink spacing increases and below which it shrinks) is a function of the applied stress as shown in Fig. 3(b). For any positive, finite stress the critical double-kink width is finite, decreasing with increasing (positive) applied stress.

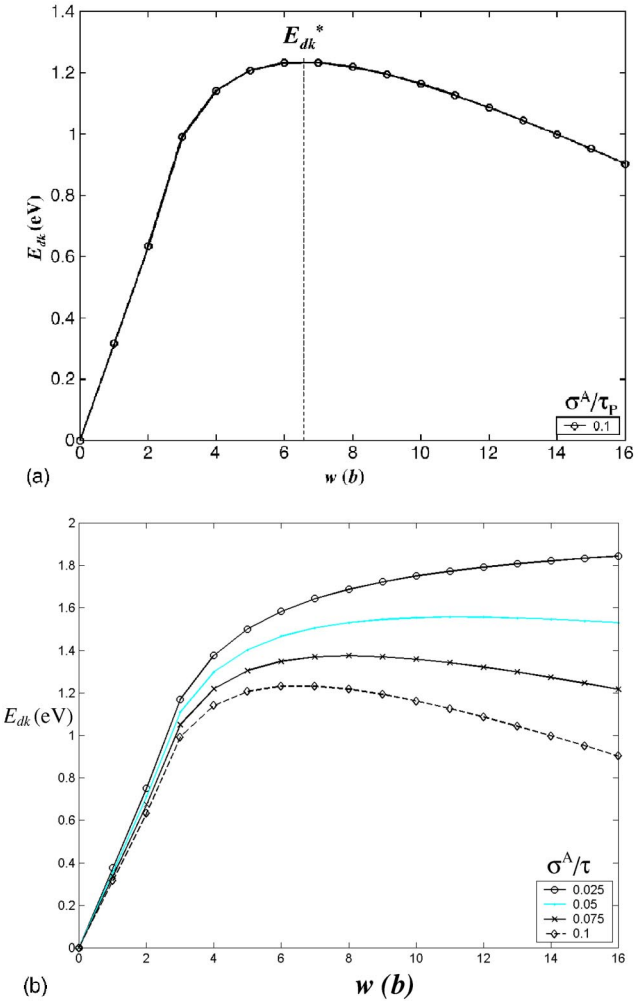

FIG. 3. (a) Variation of the double kink energy E_{dk} as a function of the width of the double kink w (separation between the two kinks) calculated using Eq. (10) and parameters described in the text. The applied stress is expressed as a fraction of the Peierls stress τ_P. (b) Variation of E_{dk} as a function of the width w (separation between the two kinks) for different values of the Peierls stress τ_P.

If a double kink is formed with a width smaller than the critical width, the two kinks attract and quickly self-annihilate. The rates of formation and self-annihilation events are so fast that the simulation would normally waste most of its time forming and annihilating subcritical double kinks. Such a problem was encountered in earlier simulations of dislocation motion.[15] The solution to this problem lies in nucleating a double kink of finite width w_0 which is at least the critical width w^* [see Fig. 3(a)], such that the double kink, once formed, is stable and embryonic nucleation events never occur. Given the importance of double-kink nucleation within the kink diffusion model, it is necessary to ensure that the calculation of the rate at which supercritical double kinks form is consistent with the real time spent forming and self-annihilating subcritical double kinks.

In order to overcome the double-kink formation and annihilation bottleneck, we employ a first-passage-time analysis that integrates over the initial evolution of the embryonic double kink by treating it as a one-dimensional random walker in double-kink width space. This approach yields the distribution of elapsed times before successful double-kink nucleation. The time distribution is obtained by applying an exact first-passage-time analysis to the one-dimensional random walk as modeled by a temporally homogenous discrete-state Markov process.[12] Details of this method can be found elsewhere.[26] Incorporation of such a double-kink nucleation model is key to efficient simulations.

Since the stress that a nucleating double kink feels varies with position along the dislocation (and time), the critical double-kink width is spatially and temporally nonuniform. The critical double-kink width is also affected by solutes that interact directly with the dislocation core through modification of the energy landscape (i.e., the solutes modify the barriers for kink motion). This effect is also incorporated in the consolidated nucleation rate using the first-passage-time analysis. Incorporation of both of these effects into the Markov chain analysis for double-kink nucleation accelerates the simulations by a factor of approximately 10^4.

F. Kinetic Monte Carlo procedure

We have described the incorporation and parametrization of the unit processes in the kink model for dislocation migration, including the effects of temperature, applied stress, solute concentration, and solute strength. We now describe the kinetic Monte Carlo implementation of this model for dislocation motion in the presence of solutes. The KMC method is similar to the *N*-fold way [or Bortz-Kalos-Lebowite (BKL) method[10]], where a variable-time increment is employed to incorporate events that occur on widely different time scales. A similar procedure was employed by Cai *et al.* to simulate dislocation motion in pure Mo (Ref. 16) and Si (Ref. 15) and by Scarle *et al.*[27] to study dislocation motion in silicon.

We extend these earlier KMC models for dislocation migration to the alloy situation (i.e., with solutes present). Initially, the glide-plane order parameter ϕ that describes the dislocation position is chosen such that there is a single screw dislocation in the glide plane. Solute atoms are distributed at random in three dimensions and represented by the solute field variable η. The simulation cell is periodic in the y and z directions (see Fig. 1). The dislocation propagates in the x direction on the $y=0$ plane. When the dislocation reaches the $+x$ boundary of the simulation cell, the simulation cell is extended in that direction by adding additional lattice points and removing the same number of lattice points from the region near the $-x$ boundary. The additional glide-plane grid points are created with the appropriate ϕ values and solute atoms are randomly placed on the new lattice points. Instead of calculating the stress on each dislocation segment due to all other segments in an infinitely repeated unit cell (in the z direction), the self-stress calculation only includes contributions from the current simulation cell, three image cells in the $+z$ direction and three image cells in the $-z$ direction.

At the beginning of each KMC step, ϕ is evaluated over the glide plane and analyzed to determine the location of each screw (horizontal) and edge (vertical) dislocation segments according to the procedure described by Eq. (5). The stress field τ_{eff} is computed at the midpoint of each dislocation segment. This stress field includes contributions from the dislocation self-stress [Eqs. (6), (7), and (8)], that associated with the solute misfit [Eq. (9)], and the externally applied stress.

In the KMC simulations, one event occurs during each step. This event is chosen based upon a sampling of all possible events that could occur, weighted by their rates (in the units of s^{-1}). These events include nucleation of double kinks and the displacement of the individual kinks. The double-kink nucleation rates (j_{DK}) are calculated from the application of the first-passage-time analysis[26] and Eq. (1) taking into account the local solute environment. The rate of kink migration depends on the distribution of solute, through the solute contribution to the stress and the direct interaction of the solute with the dislocation core. If the solute field η is zero near the kink (no solute), the migration rate (j_m) of the kinks is simply ν_k/b, where ν_k is calculated using Eq. (3). In the presence of a solute atom, there is an additional activation barrier for kink motion and j_m is calculated using Eq. (4). Kink annihilation events are treated as special cases of kink migration and are parameterized by the same set of equations [Eqs. (3) and (4)].

An event $\boldsymbol{p}$ is selected from the list of rate dependent events according to the criterion

$$\frac{\sum_{i=0}^{p-1} j_i}{R} < \xi_i < \frac{\sum_{i=0}^{p} j_i}{R}, \tag{11}$$

where R is given below by Eq. (12) and ξ_1 is a random number from [0,1). Event $\boldsymbol{p}$ involves updating ϕ over the glide plane to reflect double-kink nucleation, kink migration, or kink-kink annihilation. The normalization factor R in Eq. (11) is the sum of the rates of all possible events,

$$R = \sum_{p=1}^{N_{DK}} j_{DK}^{p} + \sum_{q=1}^{N_K} j_m^q, \tag{12}$$

where N_{DK} is the number of possible double-kink nucleation sites and N_K is the number of kink migration and annihilation events (i.e., twice the number of kinks). In the present KMC algorithm, the time increment is variable. The time increment dt is sampled from the exponential distribution of rate-dependent events as

$$dt = -\frac{\ln(\xi_2)}{R}, \tag{13}$$

where ξ_2 is a random number between [0,1) and R is the sum of the rates of all the possible events computed using Eq. (12). The procedure described above is repeated for each KMC step.

The mean dislocation position is calculated as the mean x position of all the dislocation segments, which are evaluated using the values of the parameter ϕ over the glide plane. The dislocation velocity is computed as the local slope of the

mean dislocation position versus time. In the present study, dislocation dynamics is simulated over a range of temperature, applied stress, and solute concentration.

III. MOTION OF A ⟨111⟩-ORIENTED SCREW DISLOCATION IN MOLYBDENUM AND ALLOYS

We now apply our method for simulating dislocation migration in the presence of solute to the case of the motion of a ⟨111⟩-oriented screw dislocation in bcc molybdenum alloys with up to 10% of tungsten (a substitutional solute). The Burgers vector of the dislocation is $(a_0/2)[111]$ (i.e., in the z direction). Assuming that slip occurs on the close-packed $(1\bar{1}0)$ planes (separated by $l=a_0/\sqrt{2}$), the kink height is the distance between successive $(11\bar{2})$ planes or $h=a_0/\sqrt{6}$. In an isotropic material, the interaction between a pure screw dislocation and a dilatational center of misfit (solute atom) is zero and hence the only long-range interaction between the dislocation and the solute is at the kinks, which have edge character. The difference between the lattice parameters of Mo and W is small ($\Delta a_0=0.01$ Å); hence, the strength of the dilatation field of the solute is small. In addition, the stress field associated with the solute decays quickly (as $1/r^3$).

In the Mo-W alloys considered here, the main obstruction to dislocation motion from the solute field is that associated with the interaction between the solute atoms and the dislocation core. Although this value could, in principle, be determined via *ab initio* calculations (albeit with a very large simulation cell to avoid solute-solute interactions), it has yet to be determined for the case of W in Mo. Based upon experimental measurements of the heats of segregation of various solutes to dislocations in bcc Fe,[8,28–31] we estimate the solute-dislocation core interaction energy to be in the range of 0.3 ± 0.2 eV. In the simulation results presented below we set this value at 0.3 eV. The solute-dislocation core interaction energy simply adds to the secondary Peierls barrier for dislocation motion (i.e., it modifies the activation barrier for the motion of the kinks).

In order to obtain reliable predictions of the dislocation velocities in the KMC simulations, it is essential that the kinks do not interact with their own periodic images (i.e., we must have a sufficient number of kinks on the dislocation to ensure that the kink-kink interactions are not dominated by image interactions). We perform several simulations in which we measure the dislocation velocity as a function of system size (lengths of screw dislocation), as shown in Fig. 4. These results show that the dislocation velocity increases with the system size $\mathcal{L}$ and then asymptotes to a system size-independent value at large system size. This size dependence has two origins: (i) kinks interacting with their own images and (ii) the temperature dependence of the equilibrium thermal kink separation. The minimum system size required to achieve size independent results increases with decreasing temperature and decreasing stress since lowering T and σ^A both decreases the rate of double-kink nucleation. The simulation results quoted below were all obtained using simulation cells of sufficient size to ensure that the dislocation velocity is independent of system size. Each simulation

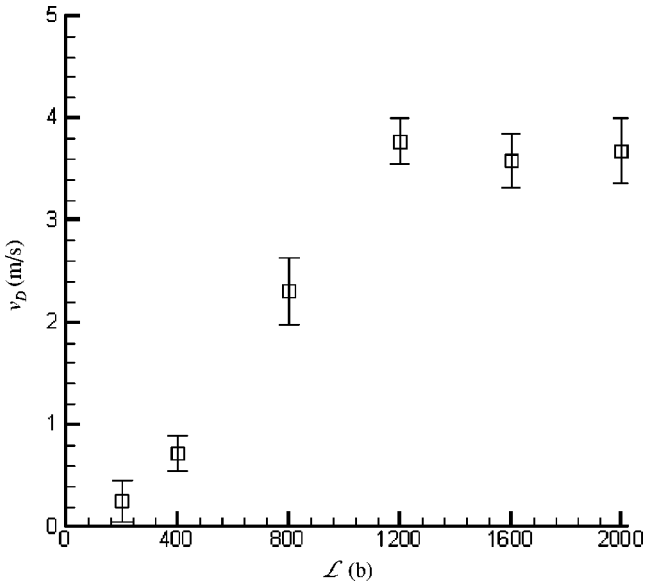

FIG. 4. Plot of the dislocation velocity as a function of system size (lengths of screw dislocation L for the same set of operational parameters). The results are independent of system size at higher system sizes.

is run for times long enough to ensure that a steady-state dislocation velocity is achieved (usually for times sufficient for the dislocation to have traveled 50–100 burgers—at least 20 mean solute spacings).

In bcc metals, the core of the screw dislocation relaxes into low-energy planar configurations. This introduces deep valleys in the Peierls energy landscape and leads to a large lattice friction to the motion of the screw dislocation. At low temperatures, the screw dislocation tends to adopt low-energy configurations and, hence, long screw dislocation segments predominate at low temperatures. In order to move a screw segment normal to itself, the dislocation core must first be constricted. Thus the energy barrier for the motion of screw dislocations and the attendant Peierls stress may be expected to be very large when compared to the energy barrier for the motion of edge dislocations. This can be seen in the values of the Peierls stress for a screw dislocation in Mo, which has been reported to be between 0.020μ and 0.025μ by several researchers[24,25,32–34] while the Peierls stress of an edge dislocation is 0.006μ. Thus, there is a large difference between the mobilities of screw and edge dislocations. Kinks on a screw dislocation are of edge character and have high mobility, but the nucleation rate of these kinks on the screw dislocation is very small, except at very high stress. Thus, the velocity of the screw dislocation should be governed primarily by the formation rate of the double kinks—i.e., double-kink formation is the rate-limiting step in the motion of screw dislocations in Mo.

Figure 5 shows the variation of the dislocation velocity (ν_D) with inverse temperature for several stresses in the range $0.04\leqslant\sigma^A/\tau_P\leqslant0.16$ in pure Mo. The velocity-temperature relationship is Arrhenius, in agreement with the analytical prediction for dislocation velocity in the kink model.[8] In contradiction to the linearizations made in most analyses of the kink model, the activation energy is a func-

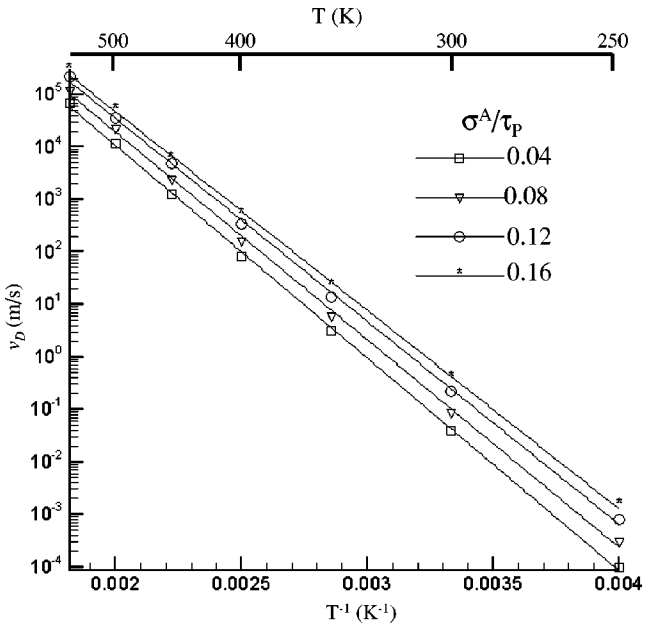

FIG. 5. Semilogarithmic plot of the dislocation velocity ν_D as a function of the inverse temperature for four different stress values for pure Mo. The corresponding temperature is shown in the bar above the plot. The applied stress is expressed as a fraction of the Peierls stress τ_P.

tion of the applied stress and decreases from 0.95 to 0.78 eV as the applied stress increases from $0.04\tau_P$ to $0.16\tau_P$. In the analytical model, the activation energy is the formation energy of a kink F_k, which in our case is 1 eV. Thus, the present simulation results are consistent with the predicted activation energy for dislocation motion (aside from the relatively weak stress dependence).

Figure 6 shows the variation of the dislocation velocity

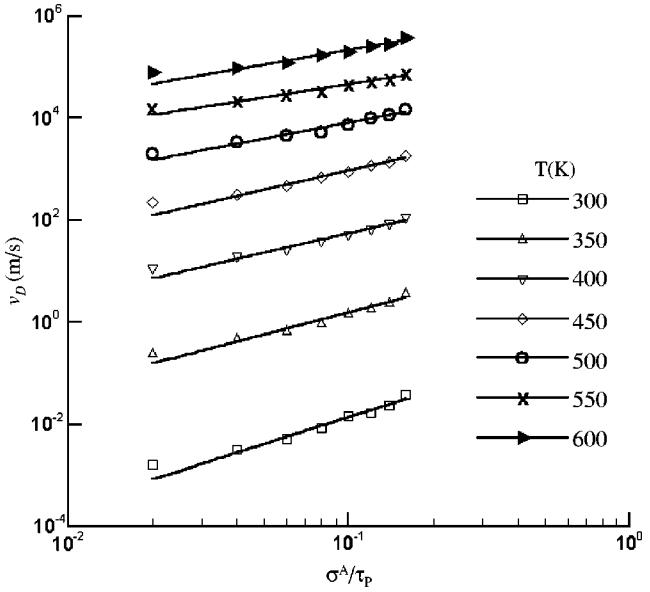

FIG. 6. Log-log plot of the dislocation velocity ν_D as a function of the applied stress σ^A at seven different temperatures for pure Mo. The applied stress is expressed as a fraction of the Peierls stress, τ_P.

with applied stress for temperatures in the range 300 K$\leqslant T \leqslant$ to 600 K. The relationship can be expressed as a power law in which the exponent decreases with temperature from 1.89 to 1.08 as the temperature increases from 300 to 600 K. While the present results can also be expressed in terms of an exponential fit, the quality of such a fit is inferior to the power law fit, especially at high stresses. Many researchers[6,7] have reported the exponents in power law fits of the dislocation velocity versus the applied stress, with the exponents varying from 0.75 to 44. Leiko and Nadgornyi[35,36] report an exponent of 7.2 from experiments on single crystals in Mo, while Prekel *et al.*[37,38] report an exponent of 6.4. There are large variations in the velocities reported by various researchers for screw dislocations in Mo, with differences in the plane of observation and high initial densities of as-grown dislocations contributing to the uncertainty in data. In light of the variability in the experimental observations and the uncertainty in the double-kink energy and kink diffusivity results employed in the present simulation, we can conclude that our results are not inconsistent with the experimental observations for screw dislocation motion in pure Mo.

While analytical predictions of the dislocation velocity in the presence of solute are possible in the framework of the kink model, such predictions have not been made for the case of alloys where the main role of the solute is as local obstacles to double kink nucleation and kink motion. Figure 7(a) shows the dependence of the dislocation velocity on temperature for solute concentrations varying from 0 (pure Mo) to 0.1 and an applied stress of $0.1\tau_P$. This figure clearly demonstrates that the activation energy for dislocation motion is very nearly unchanged by the presence of solute. The effect of solute concentration on dislocation velocity at fixed σ^A is shown in Fig. 7(b) for several temperatures. Increasing solute concentration decreases dislocation velocity at all temperatures. While the rate of decrease is very similar in all cases, the solute is more effective at reducing dislocation velocity at lower temperature. In order to view the effect of increasing solute concentration more clearly, the velocity is plotted as ν_D/ν_D^0 in Fig. 7(c), where ν_D^0 is the dislocation velocity in pure Mo. The fact that the solute is more potent at slowing the dislocations at low temperature is not surprising in light of the fact that the solute provides a barrier to critical double-kink formation. As the temperature decreases, this barrier becomes increasingly difficult to surmount and, hence, the dislocation velocity (which is proportional to the rate of double-kink production) is more strongly affected by the solute as the temperature drops.

The present observation that the effects of alloying on dislocation motion are more severe at low temperature than at high temperature is consistent with experimental observations in bcc alloys.[39–42] These experiments show that $d\sigma_y/dC_s$ increases with decreasing temperature, where σ_y is the yield stress or the critical resolved shear stress. It is interesting to note that these alloys include several cases where the solute misfit is very small (as assumed here). The fact that the same type of results are also observed for alloys in which the misfit is large suggest that the solute-dislocation core interactions may be dominant in all of these cases.

Figure 8(a) shows the variation of the dislocation velocity with applied stress in five Mo alloys at 400 K. Increasing the

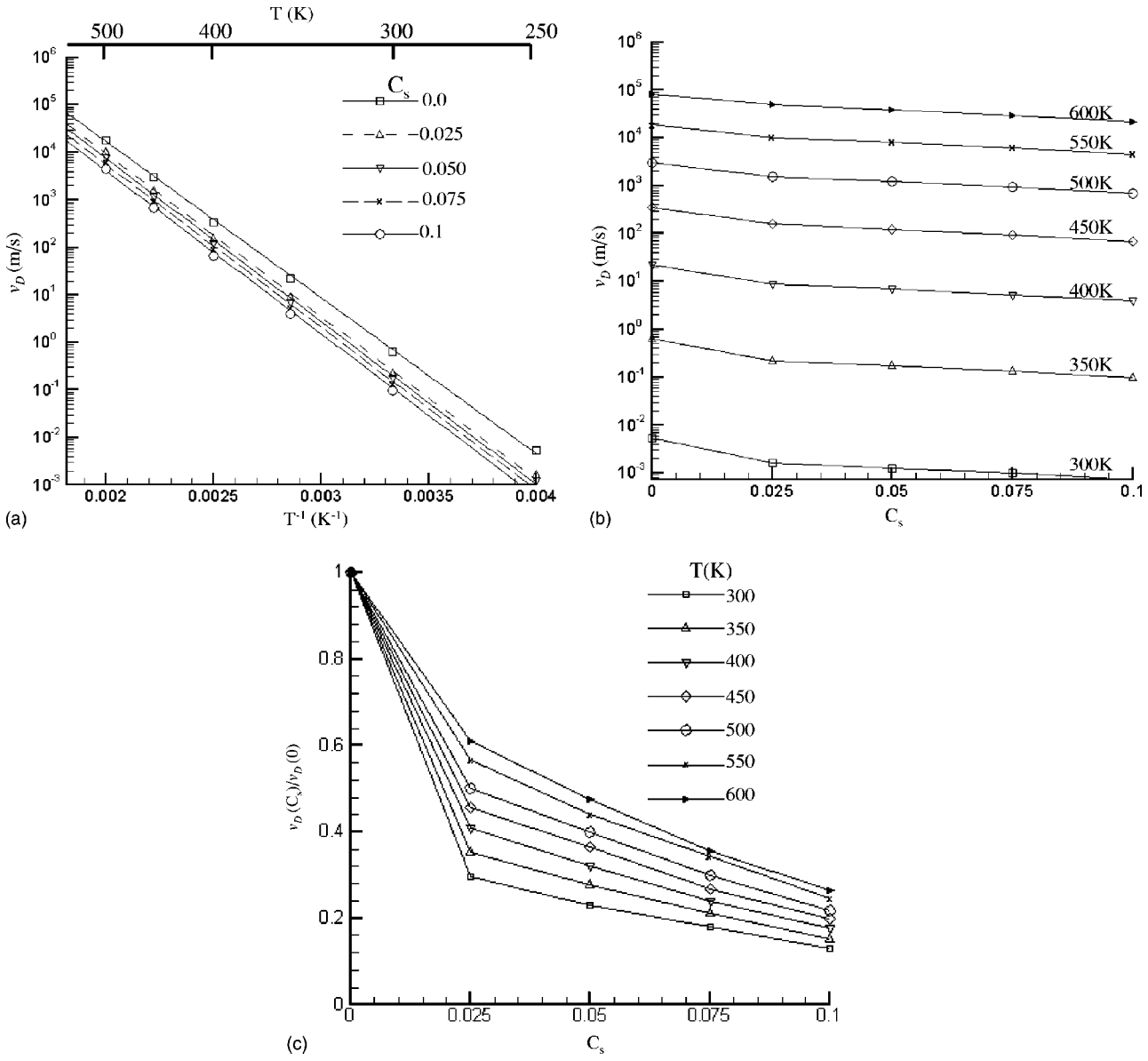

FIG. 7. (a) Semilogarithmic plot of the dislocation velocity ν_D as a function of the inverse temperature for five different alloys (varying solute concentration C_s). The corresponding temperature is shown in the bar above the plot. The applied stress is constant for all the simulations ($\sigma^A=0.1$). (b) Semilogarithmic plot of the dislocation velocity ν_D as a function of the solute concentration C_s for seven different temperatures. The applied stress is constant for all the simulations ($\tau_P=0.1$). (c) Plot of the normalized dislocation velocity as a function of the solute concentration C_s for seven different temperatures. The applied stress is constant for all the simulations ($\tau_P=0.1$). The dislocation velocity is normalized by the dislocation velocity in the pure Mo, ν_D^0.

solute concentration does not change the exponent in the velocity-stress power law, but rather decreases the prefactor. This is consistent with the observations of Leiko *et al.*,[35,36] who show that increasing the impurity concentration in Mo leads to smaller dislocation velocities but has little affect on the stress exponent. Figure 8(b) shows the same data plotted as a function of the solute concentration for different applied stresses. The effect of solute on dislocation velocity is large at very small concentration; however, further increase in the solute concentration produces a much smaller change in the dislocation velocity at all applied stresses. The same data is plotted in Fig. 8(c), with the dislocation velocity normalized by ν_D^0, the dislocation velocity in pure Mo. With this normalization, it is clear that the effect of solute on dislocation velocity is independent of the applied stress. In other words, stress and solute effects on dislocation velocity are multiplicative. This is consistent with the experimental data discussed at the end of the preceding paragraph.

IV. DISCUSSION

In the preceding section, we have shown an application of our kinetic Monte Carlo method for studying dislocation motion in bcc Mo and alloys. The results of the simulations are consistent with the analytical predictions for pure metals and with observations in bcc alloys. In light of all of the approxi-

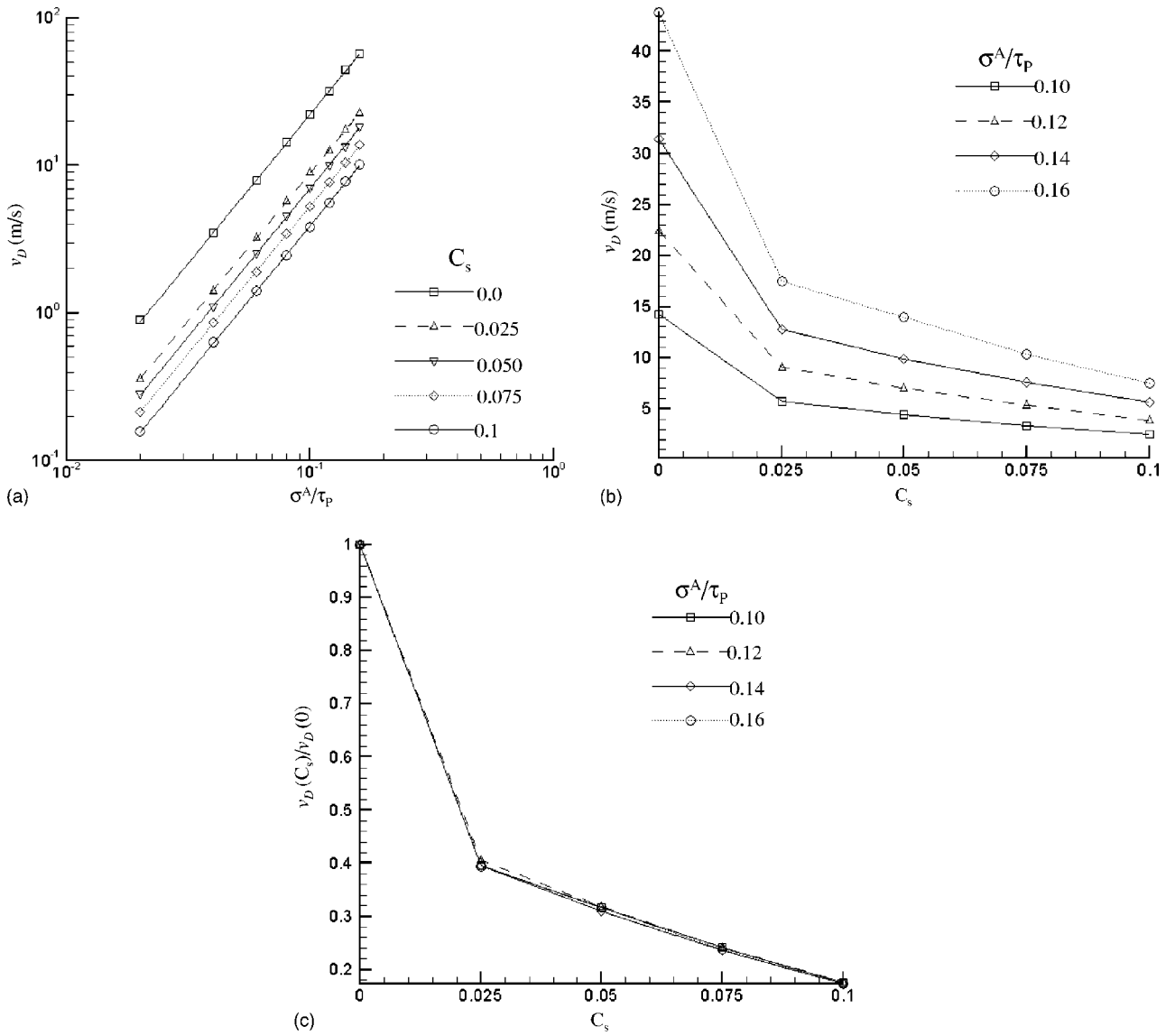

FIG. 8. (a) Semilogarithmic plot of the dislocation velocity as a function of the applied stress for five different alloys (varying solute concentration C_s). All simulations were performed at the same temperature (T=400 K). (b) Semilogarithmic plot of the dislocation velocity as a function of the solute concentration C_s for four different applied stresses at constant temperature (T=400 K). (c) Plot of the normalized dislocation velocity as a function of the solute concentration C_s for four different applied stresses at constant temperature (T=400 K). The dislocation velocity is normalized by the dislocation velocity in the pure Mo, ν_D^0.

mations made in this model and in the analytical theory, this result is nontrivial. The dislocation velocity and, hence, the strain rate are Arrhenius functions of temperature and a power law function of the applied stress. While it is not possible to directly determine the critical resolved shear stress or the yield stress directly from the results of the present simulations, we can interpret the results to understand how these quantities should vary with such factors as temperature, applied stress, and solute concentration. The activation energy for the velocity-temperature relationship is close to the formation energy of a kink and hence the rate-determining step is the formation rate of the double kinks (the diffusivity of the edge character kinks is very fast).

That the dislocation mobility is critically dependent on the nature of double-kink nucleation further underscores the importance of accurately calculating the double-kink nucleation rate. Previous KMC simulations[14,15] have made *ad hoc* assumptions regarding the calculation of the double-kink nucleation rate. The calculation of the double-kink nucleation rate by the first-passage-time method considers all possible permutations of double-kink nucleation and annihilation during the subcritical double-kink growth. It is because of this that we are able to predict dislocation velocities more accurately than heretofore possible. As an example, consider the nucleation of a double kink in the presence of a solute. The nucleation rate of the double kink depends on the distance of the solute from the double-kink nucleation site. If the solute is closer to the double-kink nucleation site, the effect of the solute on the nucleation will be much stronger. This phenomenon is properly (and automatically) accounted

for in determining the double-kink nucleation rate.

The double-kink nucleation rate and, hence, the dislocation velocity depend strongly on the applied stress, as shown in Fig. 6. The kink model should provide an accurate description of dislocation velocity above a critical stress. Hirth and Lothe[8] have estimated this critical stress to be of order $\tau_P/6$, where τ_P is the Peierls stress. In the case of molybdenum, the Peierls stress is thought to be about $0.025\tau_P$,[22,24,25,43] where τ_P is the shear modulus of Mo. This depends on the width of the kink, which increases as the applied stress increases. Thus at higher stresses, the assumption that the kinks on the dislocation are straight and narrow may no longer be valid and, hence, the double-kink energy cannot be accurately expressed via Eq. (12).

Another assumption in the model is that positively and negatively signed kinks have the same diffusivities. Recently, Bulatov *et al.*[44] showed that some asymmetry actually exists and that a multiplicity of kink structures is possible. This asymmetry with respective to positive and negative kinks may lead to differences in the kink mobility. Such an effect is not treated in this model, however, it could be easily incorporated. However, since no quantitative data exists on this effect, it was not included in the present model.

Solute-dislocation core interactions can have several different origins: solutes may be attracted to the dislocation core and dragged with the moving dislocation, may be repelled by the core, or may present static barriers to or traps for dislocation. In the example presented above, we examined a case in which the elastic interactions between dislocation and solute are weak (yet still included) and considered the main role of the solute to be the interaction of the solute with the dislocation core such that it increases the barrier to kink motion. Other mechanisms for solute dislocation interactions and their effect on dislocation mobility may be easily investigated within the framework of the present model. In particular, solutes may create a potential well in the energy landscape sampled by the moving dislocation (attractive barrier) which can trap kinks or lead to an increase in the core energy of the dislocation.[13] The present model provides a robust framework to evaluate the effects of all of these possibilities on a uniform footing. Additionally, several models for long range solute-dislocation interactions have been proposed,[28,45–48] although most follow the same approach as that employed here. The relative effects of the short-range and long-range interactions could also be investigated in more detail than we present above in our example application.

Finally, we note that there is some uncertainty in several of the parameters employed in the present calculation of the double-kink nucleation rates and the kink migration rates. The values employed here were obtained from first-principles calculations, molecular dynamics simulations, and experiments.[22,24,25,32–34] The results can be no more accurate than those parameters (we have not yet performed a sensitivity analysis on our parameter set).

The KMC simulations are closely connected to the atomistic first-principles calculations molecular-dynamics studies.[49–52] The value of the parameters determined from the atomistic studies will affect the results of the KMC simulations. We have already discussed the manner in which changes in kink diffusivity can be accomodated in the KMC simulations. Variation in the double-kink formation energy (E_{dk}) will affect the rate of nucleation and hence the time scale of the dislocation motion. Relative variation of the double-kink energy and kink migration energy may affect the transition from a nucleation-controlled motion to kink-mobility-controlled motion of the dislocation.

One of the parameters that is not accurately determined is the solute-dislocation energy E_b. Based upon experimental measurements of the heats of segregation of various solutes to dislocations in bcc Fe,[8,28–31] we estimate the solute-dislocation core interaction energy to be in the range of 0.3 ± 0.2 eV. Molecular-dynamics studies of $\langle 111\rangle$ screw dislocation interactions with solute have been performed by Farkas *et al.*[49] for Fe-Cr systems. They have employed an embedded-atom method to simulate the effect of substitutional Cr on the $\langle 111\rangle$ screw dislocation and found that the addition of excessive Cr leads to a decrease in kink mobility and consequently an increase in the Peierls stress, which is consistent with the observations of the current study. They also observed a change in the structure of the dislocation core with increasing solute concentration. Such information can be incorporated in the present KMC simulation by varying the strength of the solute-dislocation core energy parameter (E_b) with the change in the solute concentration. Based on the information provided by MD simulations of dislocation core interactions, the KMC model can be changed to incorporate the atomistic events with their kinetic and energetic parameters.

The present simulation, with its unique ability to rigorously sample relatively long time scales, can be use to provide the fundamental dislocation mobility information for more macroscopic simulation, such as the dislocation dynamics simulations which are capable of simulating the motion of a large number of dislocations.[1,2,5] Such DD simulations are used to predict overall plastic response of metals. However, all of the information on the type of material is tied up in the dislocation mobility information and a few other materials parameters. Thus the KMC simulation procedure developed here can provide a key link between the small-length and -time-scale computational methods that predict atomic properties and the larger-scale DD simulations that investigate large-scale macroscopic response metals.

V. CONCLUSION

In this paper, we have presented a kinetic Monte Carlo method for simulating dislocation motion in alloys within the framework of the kink model. The model considers the motion of a dislocation on a particular glide plane while the solute atoms are distributed in three dimensions. The model includes both a description of the short-range interaction between a dislocation core and the solute and long-range solute-dislocation interactions arising from the interplay of the solute misfit and the dislocation stress field. Double-kink nucleation rates were calculated using a first-passage-time analysis that accounts for the subcritical annihilation of embryonic double kinks as well as the presence of solutes. We explicitly consider the case of the motion of a $\langle 111\rangle$-oriented

screw dislocation on a {011}-slip plane in body-centered-cubic Mo-based alloys. Simulations were performed to determine dislocation velocity as a function of stress, temperature, and solute concentration. The dislocation velocity exhibited an Arrhenius dependence on temperature and a power law dependence on applied stress. These are consistent with some existing analytical predictions of the dependence of the dislocation velocity on these parameters. Addition of solutes decreased dislocation velocity in a manner consistent with experimental observations. The present model is very general and can be used to study dislocation motion provided that (a) the kink model is valid and (b) the fundamental properties of the dislocation and solute are known (i.e., single-kink energy, secondary Peierls barrier to kink migration, single-kink mobility, solute-kink interaction energies, solute misfit). These parameters can all be obtained from first-principles calculations and/or molecular-dynamics simulations. The method presented here provides the critical link between atomistic calculations and dislocation dynamics simulations (i.e., dislocation mobility as a function of stress, temperature, solute concentration). This link is key to the development of fully integrated models (atomistics to continuum) of the plastic deformation of alloys.

[1] V. Bulatov *et al.*, Nature (London) **391**, 669 (1998).
[2] V. Bulatov, M. Tang, and H. Zbib, MRS Bull. **26**, 191 (2001).
[3] D. Gomez-Garcia *et al.*, Revista De Metalurgia 7th National Congress on the Mechanical Properties of Solids 37, 273 (2001).
[4] M. Tang, M. Fivel, and L. Kubin, Mater. Sci. Eng., A **309**, 256 (2001).
[5] H. Zbib, T. De La Rubia, and V. Bulatov, ASME J. Eng. Mater. Technol. **124**, 78 (2002).
[6] W. Johnston and J. Gilman, Curr. Contents, Phys. Chem. Earth Sci. **28**, 12 (1979).
[7] F. R. N. Nabarro, *Theory Of Crystal Dislocations* (Clarendon Press, Oxford, 1967).
[8] J. P. Hirth and J. Lothe, *Theory Of Dislocations* (Wiley, New York, 1982).
[9] E. Nadgornyi, *Dislocation Dynamics And Mechanical Properties Of Crystals* (Pergamon Press, Oxford, 1988).
[10] A. Bortz, M. Kalos, and J. Lebowitz, J. Comput. Phys. **17**, 10 (1975).
[11] M. H. Kalos, *Monte Carlo Methods* (Wiley, New York, 1986).
[12] D. T. Gillespie, *Markov Processes: An Introduction For Physical Scientists* (Academic Press, Boston, 1992).
[13] U. F. Kocks, M. F. Ashby, and A. S. Argon, *Thermodynamics And Kinetics Of Slip* (Pergamon Press, Oxford, 1975).
[14] K. Lin and D. C. Chrzan, Phys. Rev. B **60**, 3799 (1999).
[15] W. Cai, V. Bulatov, and S. Yip, J. Comput.-Aided Mater. Des. **6**, 175 (1999).
[16] W. Cai *et al.*, Comput. Mater. Sci. **23**, 124 (2002).
[17] W. Cai *et al.*, Mater. Sci. Eng., A **309**, 270 (2001).
[18] J. Eshelby, Proc. R. Soc. London, Ser. A **266**, 222 (1962).
[19] A. Seeger, J. Phys. (Paris) **42**, 201 (1981).
[20] A. Seeger and P. Schiller, Acta Metall. **10**, 348 (1962).
[21] A. Seeger and B. Sestak, Scr. Metall. **5**, 875 (1971).
[22] W. Xu and J. A. Moriarty, Comput. Mater. Sci. **9**, 348 (1998).
[23] B. Devincre and L. P. Kubin, Mater. Sci. Eng., A **234**, 8 (1997).
[24] L. H. Yang, P. Soderlind, and J. A. Moriarty, Philos. Mag. A **81**, 1355 (2001).
[25] L. H. Yang, P. Soderlind, and J. A. Moriarty, Mater. Sci. Eng., A **309**, 102 (2001).
[26] C. S. Deo and D. J. Srolovitz, Modell. Simul. Mater. Sci. Eng. **10**, 581 (2002).
[27] S. Scarle *et al.*, in Proceedings of the 21st International Conference on Defects in Semiconductors [Physica B **308**, 493 (2001)].
[28] P. Haasen, in *Dislocations in Solids*, edited by F. R. Nabarro (North-Holland, New York, 1963), p. 155.
[29] H. Suzuki, in *Dislocations in Solids*, edited by F. R. Nabarro (North-Holland, New York, 1963), p. 191.
[30] S. Takeuchi, J. Phys. Soc. Jpn. **27**, 929 (1969).
[31] S. Takeuchi, H. Yoshida, and T. Taoka, Trans. Jpn. Inst. Met. **S 9**, 715 (1968).
[32] S. Rao and C. Woodward, Philos. Mag. A **81**, 1317 (2001).
[33] C. Woodward and S. Rao, Philos. Mag. A **81**, 1305 (2001).
[34] S. Ismail-Beigi and T. Arias, Phys. Rev. Lett. **84**, 1499 (2000).
[35] E. B. Leiko *et al.*, Fiz. Tverd. Tela (Leningrad) **17**, 2735 (1975).
[36] E. B. Leiko and E. M. Nadgorny, Kristallografiya **19**, 584 (1974).
[37] H. L. Prekel and H. Conrad, Acta Metall. **15**, 955 (1967).
[38] H. L. Prekel, A. Lawley, and H. Conrad, Acta Metall. **16**, 337 (1968).
[39] J. W. Christian and B. C. Masters, Proc. R. Soc. London, Ser. A **281**, 223 (1964).
[40] J. W. Christian and B. C. Masters, Proc. R. Soc. London, Ser. A **281**, 240 (1964).
[41] T. E. Mitchell and P. L. Raffo, Can. J. Phys. **45**, 1047 (1967).
[42] P. L. Raffo and T. E. Mitchell, Trans. Metall. Soc. AIME **242**, 907 (1968).
[43] M. S. Duesbery and V. Vitek, Acta Mater. **46**, 1481 (1998).
[44] V. Bulatov, J. Justo, W. Cai, and S. Yip, Phys. Rev. Lett. **79**, 5042 (1997).
[45] R. Labusch, Acta Metall. **20**, 917 (1972).
[46] R. Labusch, Czech. J. Phys., Sect. B **31**, 165 (1981).
[47] R. L. Fleischer, Acta Metall. **9**, 996 (1961).
[48] R. L. Fleischer, J. Appl. Phys. **33**, 3504 (1962).
[49] D. Farkas *et al.*, Acta Mater. **44**, 409 (1996).
[50] J. P. Chang *et al.*, Mater. Sci. Eng., A **309**, 160 (2001).
[51] J. Chang *et al.*, Comput. Mater. Sci. **23**, 111 (2002).
[52] S. Nedelcu and P. Kizler, Phys. Status Solidi A **193**, 26 (2002).